

https://dspace.org/

Free convection of CattaneoChristov heat flux model for the micropolar hybrid nanofluid through permeable stretching surface with inertial drag and irregular heat sinksource

Titilayo Agbaje; S Panda; S Mishra; R Baithalu

https://hdl.handle.net/10539/47313
WOS

Downloaded from a DSpace repository. https://dspace.org/

Multiscale and Multidisciplinary Modeling, Experiments and Design (2025) 8:184
https://doi.org/10.1007/s41939-025-00768-5

ORIGINAL PAPER

Free convection of Cattaneo-Christov heat flux model for the micropolar hybrid nanofluid through permeable stretching surface with inertial drag and irregular heat sink/source

Titilayo M. Agbaje[1] · Subhajit Panda[2] · S. R. Mishra[3] · Rupa Baithalu[3]

Received: 17 December 2024 / Accepted: 25 January 2025 / Published online: 17 February 2025
© The Author(s), under exclusive licence to Springer Nature Switzerland AG 2025

Abstract
The advanced cooling technologies, biomedical engineering and in different energy systems heat transfer presents its pivotal role. In this regard, micropolar fluid has a significant contribution due to its vast applications. The present study explores the free convection behavior of a micropolar hybrid nanofluid, using water as the base liquid and incorporating diamond and copper as the solid nanoparticles. Additionally, the thermal relaxation effect is accounted for by the inclusion of Cattaneo-Christov heat flux in the energy equation and the impact of Darcy-Forchheimer inertial drag with an irregular heat sink/source. In particular, the non-Newtonian behavior with rotational effect and Couple stress is crucial for the flow in micropolar fluids is highly relevant for applications in cooling systems for microelectronics. The dimensional complex system is converted into a corresponding non-dimensional form with a suitable choice of similarity rules. The flow profiles equipped with different phenomena are solved utilizing the spectral quasi-linearization method. The effective properties of several contributing factors likely, micropolarity, thermal relaxation, magnetic, porosity, inertial drag, particle concentration, non-uniform heat source/sink, etc. are presented through graphs and elaborated via validation and convergence of the methodology used in this article. The results highlight the interaction between thermal relaxation and micro-channel effects demonstrating heat transfer capabilities of the hybrid nanofluid. Further, the heat transfer rate enhances for the higher thermal radiation and the impact is reversed for the enhanced heat source along with thermal relaxation parameter.

Keywords Hybrid nanofluid · Micropolar fluid · Cattaneo-Christov heat and mass flux model · Irregular heat sink/source · Spectral quasilinearization method

1 Introduction

Micropolar fluids are complex fluids that exhibit microstructure and are characterized by the presence of micro-rotational effects and couple stresses. Unlike classical Newtonian fluids, which assume that the fluid particles have no internal structure, micropolar fluids consider the particles as rigid bodies that can undergo rotational motion. Micropolar fluids find diverse applications across various fields due to their distinctive properties that consider micro-rotational effects and couple stresses. The consideration of both the fluid and vortex viscosity makes them usually used in various applications in cooling of electronic devices, peristaltic pumping processes, and other systems that use dissipative heat impact, etc. more specifically, in manufacturing industries, the polymer extrusion processes, the use of polar fluid is crucial. The wide use of lubricating systems in mechanical engineering to avoid roughness, particularly in journal bearings, these fluids are

✉ S. R. Mishra
satyaranjan_mshr@yahoo.co.in

Titilayo M. Agbaje
titilayoagbaje@gmail.com

Subhajit Panda
spanda.math@gmail.com

Rupa Baithalu
rupadhananjaygarnaik@gmail.com

[1] School of Computer Science and Applied Mathematics, University of the Witwatersrand, Private Bag 3, Braamfontein, Johannesburg 2050, South Africa

[2] Centre for Data Science, Department of Computer Science and Engineering, Siksha 'O' Anusandhan Deemed to be University, Bhubaneswar, Odisha 751030, India

[3] Department of Mathematics, Siksha 'O' Anusandhan Deemed to be University, Bhubaneswar, Odisha 751030, India

useful in enhancing their consistent performance. Abdel et al. (2024) carried out the study of entropy formation considering a wavy channel filled with polar fluid under the action of velocity slip as well as convective thermal conditions and slip flow. Furthermore, an approximate analytical technique with the help of the perturbation technique is utilized for the solution of the flow profiles. Finally, the result revealed the impact of several parameters that are useful in enhancing the entropy analysis within the system. Further, the motion of Sutterby micropolar fluid via an exponentially expanding bended surface for the impact of a chemical reaction is proposed by Abbas et al. (2024a). A traditional numerical technique is utilized for the solution of transformed standard equations with the help of several characterizing factors. The examination of the impact of magnetization and the reacting agents are briefly discussed. Recently, the analysis of an electrically conducting flow of polar fluid for the inclusion of SWCNT solid nanoparticles immersed in water is presented by Panda et al. (2024). Moreover, the characteristic of the radiative heat along with the interaction of magnetization within a porous matrix enhances the flow behavior. Moreover, the assumption of the Gherasim viscosity model and Hamilton-Crosser conductivity model are useful in defining the shape factor of various nanoparticles on the flow properties. To ensure the optimized heat transport properties, an innovative statistical approach is utilized i.e. involving both suction and injection. However, optimizing shear drag rate analysis on the H_2O-based CNT polar fluid is organized by Baithalu and Mishra (2023a). The flow over an expanding surface with the interaction of diversified factors is obtained graphically and explained briefly. Again, Baithalu and Mishra (2023b) proposed the role of magneto-micropolar fluid for the interaction of thermal buoyancy vis-à-vis the impact of radiating heat and chemical reactions. Also, the focus of the study is the interaction of applied transverse magnetism, for the variation of the Peclet number influences the flow profiles. Finally, "*Differential Transform Method (DTM)*" an approximate analytical technique is presented for the solution of the flow model. transformed model Pattnaik et al. (2024) focused on the 2D circulation of a conducting polar nanofluid within a parallel channel equipped with permeable medium. Additionally, the flow is influenced by various physical factors, including thermal buoyancy, radiative heat, and substantial heat supplier, which enhance the flow profiles. Furthermore, the coupled nonlinear transformuted equations are solved numerically with the interaction of several factors.

The combined effect of two or more solid nanoparticles i.e., hybrid nanofluids are advanced thermal fluids, resulting in enhanced thermal properties compared to conventional fluids. Due to enhanced thermal conductivity and efficiency in the heat transfer properties it is widely used in several applications such as in industrial processes, in heat exchangers, refrigeration, where efficient thermal management is crucial. In the automotive industry, they improve the cooling efficiency of engines and battery systems, leading to better performance and energy efficiency. Additionally, hybrid nanofluids are employed in solar energy systems to enhance the absorption and transfer of heat, significantly improving the efficiency of solar collectors, targeted therapies. Memon et al. (2024) explored the laminar MHD 2D Darcy-Forchheimer model combined with micropolar water-based hybridised (Cu + MoS2) nanofluids, on porous surfaces are considered. Simultaneously, the governing PDEs are derived using the "Tiwari-Das model". Further, the transformed model is handled numerically with the shooting approach in Maple, revealing dual solutions. Alamarashi et al. (2024) analyzed a non-Newtonian micropolar time-dependent hybrid nanofluid, with the interaction of thermal radiation over a radially rotating disc. The specialty of the proposed model is due to the interaction of both Darcy and Forchheimer's assumptions. The impact of magnetization along with dissipative heat using Joule and Darcy dissipation. Aldhafeeri and Yasmin (2024) have presented the impact of nanoparticles in water to analyze the 2D, magnetised hybridised micropolar fluid flow via a permeable interface composed within a permeability. Additionally, the "Cattaneo-Christov heat and mass flux model" is employed to evaluate the energyy and solutal diffusion in thermal and concentration field. A semi-analytical approach known as the "*Homotopy Analysis Method (HAM)*" is applied, utilizing MATHEMATICA software for analytical analysis of the nonlinear ODEs. Usafzai and Aly (2022) presented the impact of velocity slip on the micropolar hybrid nanofluid considering Cu and Al_2O_3 as nanoparticle in water through a permeable expanding surface. They have imposed both the PST and PHF temperature conditions in the heat transport phenomenon. The exact solutions for the flow phenomena are obtained and then they have employed analytical approach for the solution of transformed main equations. The effects of various physical phenomena such as thermal radiation along with cross-diffusion, and the applied magnetic field on the movement of highly micropolar hybridised fluid is explored by Upadhya et al. (2022). Furthermore, the total entropy analysis for the process of irreversibility within the system was also examined for the energy transportation rate. Additionally, the flow equations are modelled through a curvilinear system, and suitable similarity function are employed to convert the standard nonlinear PDEs into ODEs. The proposed system is then numerically solved through a "*fourth-order Runge–Kutta method*" along with a shooting procedure. Vidyarani et al. (2024) inspected the impact of "*Cattaneo–Christov heat and mass flux*" on the swirling flow across a stretchable cylinder. The Navier–Stokes equation is used to model the anticipated flow in the development of this mathematical model. Similarity functions are applied to renovate the system into

a set of ODEs. The "*Runge–Kutta-Fehlberg 45 (RKF-45) method*" is then implanted to analyze the resulting dimensionless system. With the use of generalised conservation principles and the "Cattaneo-Christov heat and mass flux theory", Madkhali et al. (2024) seek to improve the transmission of energy and mass in a tri-nanofluid via an extended surface. Moreover, the formulated problems are addressed through a "*Finite Element Method (FEM)*". Eid et al. (2024) considered the effects of Ohmic heating, nonuniform heat supplier on the flow and energy transmission of power-law non-Newtonian fluids via an expanding surface within a porous substance, using the "Cattaneo-Christov model (CCM)". Finally, the non-linear ODEs are numerically solved via the "Runge–Kutta method" with a shooting procedure. Ramzan et al. (Ramzan et al. 2024) considered the energy and mass transportation features of Casson nanoliquid motion through a bended elastic surface, incorporating the Cattaneo-Christov heat flux model. In their work the numerical solution is obtained using the "Homotopy Analysis Method (HAM)". Additionally, the accurateness of the model is authenticated through a comprehensive comparison with existing published results. A third-grade MHD fluid with the inclusion of "Cattaneo–Christov model" is considered by Rehman et al. (Rehman et al. 2023a) in investigating the effect of thermal relaxation utilizing heat flux over an expanding surface. It determines the heat transmission properties with the impact of thermal relaxation time and computes the normal stress components those are not considered in second-grade models. Additionally, the role of Soret and Dufour is described by the use of cross diffusion effect. Furthermore, Rehman et al. (2023b) proposed the flow characteristics of Jeffery-Hamel motion among non-parallel convergent-divergent channels by incorporating thermal relaxations time. The mathematical simulation of the flow problem led to the construction of governing PDEs that incorporate a range of different factors.

The "Spectral Quasilinearization Method (SQLM)" is an advanced technique for solving nonlinear differential equations by integrating spectral methods with a quasilinearization strategy. This method approximates solutions using a series expansion with orthogonal functions like Fourier series or Chebyshev polynomials. It simplifies nonlinear problems by iteratively linearizing them around an initial approximation, with each iteration refining the solution until it converges to the exact result. The spectral aspect ensures high accuracy by efficiently representing the solution and its derivatives through orthogonal functions. SQM is particularly useful for tackling complex boundary value problems and nonlinear partial differential equations across various domains, including fluid dynamics, heat transfer, and applied mathematics, providing both precision and computational efficiency. Mishra et al. (2024) and Baithalu et al. (2024) explored the analysis of entropy utilizing hybrid nanofluid containing CNT particles for efficient heat transfer applications. The governing equations equipped with various flow properties are handled numerically by employing the multivariate spectral quasilinearization method. The same methodology was adopted by Goqo et al. (2019) in examining the motion of electrically conducting nanoliquid within a square cavity embedding porous medium. Further, the accuracy as well as the efficiency of the model is obtained by validating their work with earlier studies. Spectral methods have been the subject of substantial study and development by numerous researchers (Bellman and Kalaba 1965; Canuto et al. 1988), who have made major contributions to a wide range of scientific and engineering domains. Numerous investigators (Mishra et al. 2016; Mohapatra et al. 2024; Panda et al. 2023; Shamshuddin et al. 2024) have carried out comprehensive investigations into the movement of micropolar liquids in diverse geometries. In this study, the influence of ferromagnetic nanoparticles on the behavior of Williamson fluid is analysed by Khan (2023). Suitable similarity transformations are applied to reduce the governing equations to a system of nonlinear ordinary differential equations (ODEs). Additionally, the velocity and thermal gradients are examined and presented graphically for detailed analysis. Khan et al. (2022) investigated the heat and mass transfer properties of an incompressible Sutterby nanofluid flowing over a stretching, non-porous surface. Additionally, the effects of Brownian motion and thermophoresis are considered. To simplify the analysis, similarity transformations are applied to convert the coupled PDEs into a system of coupled ODEs which are then solved numerically using the efficient bvp4c method. Khan et al. (2022) explored on analyzing the 2D flow of a modified Eyring-Powell model under the influence of a magnetic field. Additionally, the activation energy phenomenon is examined. This phenomenon is characterized by hydrodynamic instability and pattern formation within suspensions of swimming microbes. The governing coupled partial differential equations (PDEs) are transformed into a system of ODEs and solved using the bvp4c numerical scheme. The results are then compared with those obtained using the "Homotopy Analysis Method (HAM)" for validation. Khan et al. (2022) developed to study the heat sink/source-based Sutterby liquid flow under the influence of thermophoretic and Brownian motion within a wedge geometry. By applying appropriate similarity transformations, the governing partial differential equations (PDEs) are reduced to a system of ordinary differential equations (ODEs). These coupled ODEs are solved numerically using the MATLAB bvp4c solver. The thermal and concentration distributions are analyzed and presented graphically. The results indicate that the temperature field increases with the Brownian motion parameter, while the concentration field decreases. Khan et al. (2020) studied the heat sink-source and melting phenomena in the time-dependent Falkner–Skan flow of Cross nanofluid, while also considering stagnation

point flow characteristics. Using the boundary layer concept, the compact form of the Cross fluid equations is converted into component form, and appropriate transformations are employed to derive a system of ordinary differential equations (ODEs). The resulting ODEs are solved numerically. Abbas et al. (2024b) examined the effects of viscous dissipation on the stagnation point flow of a trihybrid nanofluid (THNF) under the influence of Marangoni convection and activation energy. Additionally, the impact of heat generation and magnetic field is considered. Moreover, it holds promise in biomedical engineering, particularly for targeted drug delivery, where controlled fluid flow enables precise transport of therapeutic agents. It is also relevant in the design of lab-on-a-chip technologies and microfluidic devices, where understanding fluid behavior at the microscale is essential. A set of nonlinear ordinary differential equations (ODEs) is derived from the governing equations of the problem using similarity techniques. These resulting equations are solved numerically using the shooting method. Abbas et al. (2024c) explored the thermo-solutal Marangoni convection effects on the Darcy-Forchheimer stagnation point flow of a magnetohydrodynamic (MHD) tetra-hybrid nanofluid around a rotating sphere, considering activation energy. Elboughdiri et al. (2024) examined the impact of Soret and Dufour effects on the three-dimensional (3D) flow of trihybrid nanofluid (THNF) over a sheet within a porous medium, incorporating heat radiation and Stefan blowing effects. Additionally, an advanced approach for 3D analysis of THNF flow under Stefan blowing is presented in the current investigation. Abbas et al. (2024d) explored a study is to investigate the enhancement of thermal energy transfer in the flow of Ellis THNF influenced by magnetic dipole effects on a vertical surface. The analysis considers the dynamics of flow, mass, and heat transfer, incorporating the effects of Marangoni convection and the Cattaneo-Christov mass and heat flux model. Faisal et al. (2024a, 2024b) examined on evaluating entropy in the bi-directional flow of Casson hybrid nanofluids within a stagnated domain, a key topic for optimizing thermal systems. The objective is to analyze the behavior of unsteady, magnetized, and laminar flow using a parametric model based on the thermo-physical properties of alumina and copper nanoparticles. Dharmaiah et al. (2023) explored the flow and heat transfer characteristics in the boundary layer to understand the behavior of a porous exponentially stretched sheet. Numerical solutions to these equations are obtained using the Runge–Kutta-Fehlberg method combined with the shooting technique.

Research gaps with objectives: Following above mentioned studies several lacking is observed those are not explored showing the research gaps.

- The study of hybrid nanofluid using diamond and Cu nanoparticles is unexplored in the case of micropolar fluid especially for the interaction of the Cattaneo-Christov model therefore present investigation fulfils this as a major objective.
- Earlier investigation has lack in the discussion of inertial drag with an irregular heat sink/source with micropolarity which is included in the current case of hybrid nanofluid.
- Traditional investigations have not focused much more on the solution of using SQLM for the hybrid nanofluid with the interaction of radiating energy and other properties through a permeable medium, which is explored in the current investigation.
- Existing literature does not focus on the thermal relaxation with space and temperature dependent heat sink/source that is more effectively visualized now.

Approaches leading to the novelty: Certain considerations as well as assumptions made in this article lead to the novelty of the proposed investigation and these are;

- The integration of Cattaneo-Christov heat flux model with the polarity of the micropolar hybrid nanofluid provides constructive ideas for the thermal relaxation effects.
- The utility of the diamond and Cu nanoparticles jointly with base liquid water performs its greater ability for their effective properties through a permeable medium over a stretching sheet.
- Examining the impact of non-uniform heat sources/sinks, i.e., the impact of space and temperature-dependent heat sources/sinks in the presence of drag, provides advanced cooling and energy systems.
- The application of the spectral quasilinearization method to solve the boundary value problem for micropolar hybrid nanofluid shows a novel approach over other existing methods.

2 Mathematical modelling

A Darcy-Forchheimer free convective MHD micropolar hybridized nanofluid comprised of Diamond and Copper nanoparticles in water over a vertical porous stretching sheet is analyzed in this article. Additionally, the heat transport phenomenon enriches due to the inclusion of the Cattaneo-Christov model associated to the impact of thermal radiation. Further, the interaction of non-uniform heat source combined with characterizing parameter enhances the flow properties. The coordinate axes based on the main flow of the fluid (u) towards the x direction and the transverse flow (v) acting along y direction. Here, $u_w = ax$ is the assumption of linear stretching velocities of the surface. Moreover, the sheet and the ambient temperature are assumed to be Tw and T∞ respectively. A magnetic strength B_0 of the magnetized field

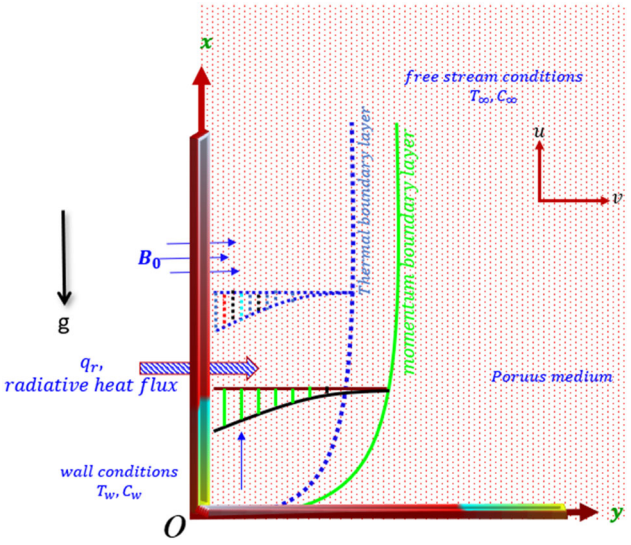


Fig. 1 Flow geometry

is imposed along the transverse direction of the main flow (Fig. 1). Following the afore-mentioned assumption the governing flow problems are described as;

Under the aforementioned presumptions, the following is a list of the mathematical formulations for standard equations Panda et al. (2024):

$$\frac{\partial u}{\partial x}+\frac{\partial v}{\partial y}=0 \tag{1}$$

$$\rho_{hnf}\left(u\frac{\partial u}{\partial x}+v\frac{\partial v}{\partial y}\right)=\left(\mu_{hnf}+\kappa\right)\frac{\partial^2 u}{\partial y^2}+\kappa\frac{\partial N}{\partial y} - \sigma_{hnf}B_0^2u-\frac{\mu_{hnf}}{k_p}u + g\left(\rho\beta\right)_{hnf}\left(T-T_\infty\right)-\frac{C_b}{x\sqrt{k_p}}u^2 \tag{2}$$

$$\rho_{hnf}\left(u\frac{\partial N}{\partial x}+v\frac{\partial N}{\partial y}\right)=\frac{\chi_{hnf}}{j}\frac{\partial^2 N}{\partial y^2}-\frac{\kappa}{j}\left(2N+\frac{\partial u}{\partial y}\right) \tag{3}$$

$$\left(\rho Cp\right)_{hnf}\left(u\frac{\partial T}{\partial x}+v\frac{\partial T}{\partial y}\right) -\lambda\left[\begin{array}{l} v\frac{\partial T}{\partial y}\frac{\partial v}{\partial y}+u^2\frac{\partial^2 T}{\partial x^2}+v^2\frac{\partial^2 T}{\partial y^2}+u\frac{\partial T}{\partial x}\frac{\partial u}{\partial x} \\ +2uv\frac{\partial^2 T}{\partial x\partial y}+u\frac{\partial T}{\partial y}\frac{\partial v}{\partial x}+v\frac{\partial T}{\partial x}\frac{\partial u}{\partial y}\end{array}\right] =k_{hnf}\frac{\partial^2 T}{\partial y^2}-\frac{\partial q_r}{\partial y}+q''' \tag{4}$$

The adopted surface conditions for the proposed model are:

$$\left.\begin{array}{l} u=u_w=ax,\ v=0,\ N=-n\frac{\partial u}{\partial y},\ T=T_w,\quad at\ y=0, \\ u\to 0,\ v\to 0,\ N\to 0,\ T\to T_\infty,\qquad as\ y\to\infty.\end{array}\right\} \tag{5}$$

where $q'''=\left(\frac{kU_w(x)}{x\upsilon}\right)\left[A^*(T_w-T_\infty)f'(\eta)+B^*(T-T_\infty)\right]$.

Here, the irregular heat supplier partially split into space-dependent (A^*) and temperature dependent (B^*) heat sink/source successively. In particular, the positive sign indicates the heat generation and the negative sign represents the heat absorption.

The boundary conditions presented in Eq. (5) reflects the surface velocity is linear ($u_w=ax$), the surface is impermeable ($v=0$), Tw is the surface temperature and the ambient state conditions.

The nonlinear heat flux can be expressed in linear form as;

$$q_r=-\frac{16\sigma^*T_\infty^3}{3k^*}\frac{\partial T}{\partial y} \tag{6}$$

Currently, establish the subsequent similarity transformation

$$\left.\begin{array}{l} \psi=\sqrt{a\upsilon}xf\left(\eta\right),\ u=axf'\left(\eta\right), \\ v=-\sqrt{a\upsilon}f\left(\eta\right),\ N=a\sqrt{a/\upsilon}xh\left(\eta\right), \\ \theta\left(\eta\right)=\frac{\left(T-T_\infty\right)}{\left(T_w-T_\infty\right)},\ \eta=y\left(\frac{a}{\upsilon}\right)^{\frac{1}{2}}\end{array}\right\} \tag{7}$$

One has

$$\frac{1}{A_2}\left(A_1+K\right)f'''-f'^2+ff'' +\frac{1}{A_2}\left(Kh'-A_3Mf'-A_1Kpf'\right) +\frac{A_4}{A_2}Gr\theta-Frf'^2=0 \tag{8}$$

$$\frac{1}{A_2}\left(A_1+\frac{K}{2}\right)h''-\frac{K}{A_2}\left(2h+f''\right)+fh'-f'h=0 \tag{9}$$

$$\left(A_5+\frac{4}{3}Rd\right)\theta'' +\Pr A_6\left(\Omega\left(ff'\theta'+f^2\theta''\right)+f\theta'\right) +Af'+B\theta=0 \tag{10}$$

$$\left.\begin{array}{l} f(0)=0,\ f'(0)=1,\ h(0)=-nf''(0),\ \theta(0)=1, \\ f'(\infty)\to 0,\ h(\infty)\to 0,\ \theta(\infty)\to 0,\end{array}\right\} \tag{11}$$

where the non-dimensional factors used in the governing transmuted equations are

$$\left.\begin{aligned} &\mathrm{Pr}=\frac{\upsilon_f}{\alpha_f},\ Rd=\frac{4\sigma^* T_\infty^3}{k_f k^*},\ M=\frac{\sigma B_0^2}{\rho_f a},\ Gr=\frac{g\beta(T_w-T_\infty)x^3}{\upsilon^2}\\ &K=\frac{\kappa}{\mu_f},\ Kp=\frac{\upsilon_f}{ak_p},\ \Omega=a\lambda,\ Fr=\frac{C_b}{\sqrt{k_p}}, \end{aligned}\right\} \tag{12}$$

$$\begin{aligned} &A_1=\frac{\mu_{hnf}}{\mu_f},\ A_2=\frac{\rho_{hnf}}{\rho_f},\ A_3=\frac{\sigma_{hnf}}{\sigma_f},\\ &A_4=\frac{(\rho\beta)_{hnf}}{(\rho\beta)_f},\ A_5=\frac{k_{hnf}}{k_f},\ A_6=\frac{(\rho Cp)_{hnf}}{(\rho Cp)_f} \end{aligned}$$

The physical models for the nanofluid and the hybrid nanofluids are depicted in Table 1 and the thermal properties are displayed in Table 2.

2.1 Quantities related to physical interest

Drag forces at surface

We have

$$Cf_x=\frac{\tau_w}{\frac{1}{2}\rho_f U_w^2},\ Nu_x=\frac{xq_w}{k_f(T_w-T_\infty)}, \tag{13}$$

where

$\tau_w=\left(\left(\mu_{hnf}+K\right)\frac{\partial u}{\partial y}\right),\ q_w=k_{hnf}\left(-\frac{\partial T}{\partial y}\right)+q_r\Big|_{at\ y=0}$, are the sheer stress and surface heat flux.

Therefore Eq. (18) can be described as:

$$\begin{aligned} &Cf_x=\frac{1}{\rho_f U_w^2}\left(\left(\mu_{hnf}+K\right)\frac{\partial u}{\partial x}\right)\Big|_{y=0},\\ &Nu_x=\frac{xk_{hnf}}{k_f(T_w-T_\infty)}\left(-\frac{\partial T}{\partial y}\right)+q_r\Big|_{y=0}, \end{aligned} \tag{14}$$

Implementing the similarity variables we get:

$$\begin{aligned} &(\mathrm{Re}_x)^{1/2}Cf_x=2(A_1+K)f''(0),\\ &(\mathrm{Re}_x)^{-1/2}Nu_x=-\left(A_5+\frac{4}{3}Rd\right)\theta'(0) \end{aligned} \tag{15}$$

3 Method of solution

The nonlinear ordinary differential Eqs. (8)–(10) and the constraints on the boundary (11), given the noteworthy nonlinearity in the framework characterising the phenomena, are numerically resolved employing the "spectral quasilinearization method (SQLM)". This technique is used over several overlapping time periods. The "*quasilinearization*

Table 1 Significant models of hybrid nanofluid

Thermophysical properties	Hybrid nanofluid
Density	$\frac{\rho_{hnf}}{\rho_f}=\frac{(1-\phi_2)\left[(1-\phi_1)\rho_f+\phi_1\rho_{s1}\right]+\phi_2\rho_{s2}}{\rho_f}$
Heat capacity	$\frac{(\rho Cp)_{hnf}}{(\rho Cp)_f}=\frac{\phi_2(\rho Cp)_{s2}+(1-\phi_2)\left[(1-\phi_1)(\rho Cp)_f+\phi_1(\rho Cp)_{s1}\right]}{(\rho Cp)_f}$
Thermal expansion	$\frac{(\rho\beta)_{hnf}}{(\rho\beta)_f}=\frac{\phi_2(\rho\beta)_{s2}+(1-\phi_2)\left[(1-\phi_1)(\rho\beta)_f+\phi_1(\rho\beta)_{s1}\right]}{(\rho\beta)_f}$
Viscosity	$\frac{\mu_{hnf}}{\mu_f}=\frac{1}{(1-\phi_1)^{2.5}(1-\phi_2)^{2.5}}$
Thermal conductivity	$\frac{k_{hnf}}{k_{nf}}=\frac{k_{s2}+(n-1)k_{nf}-(n-1)\phi_2\left(k_{nf}-k_{s2}\right)}{k_{s2}+(n-1)k_{nf}+\phi_2\left(k_{nf}-k_{s2}\right)}$ $\frac{k_{nf}}{k_f}=\frac{k_{s1}+(n-1)k_f-(n-1)\phi_1\left(k_f-k_{s1}\right)}{k_{s1}+(n-1)k_f+\phi_1\left(k_f-k_{s1}\right)}$
Electrical conductivity	$\frac{\sigma_{hnf}}{\sigma_{nf}}=\frac{\sigma_{s2}+(n-1)\sigma_{nf}-(n-1)\phi_2\left(\sigma_{nf}-\sigma_{s2}\right)}{\sigma_{s2}+(n-1)\sigma_{nf}+\phi_2\left(\sigma_{nf}-\sigma_{s2}\right)}$ $\frac{\sigma_{nf}}{\sigma_f}=\frac{\sigma_{s1}+(n-1)\sigma_f-(n-1)\phi_1\left(\sigma_f-\sigma_{s1}\right)}{\sigma_{s1}+(n-1)\sigma_f+\phi_1\left(\sigma_f-\sigma_{s1}\right)}$

Table 2 Properties relating to numerical results of materials (Panda et al. 2024)

Base fluid and nanoparticle	$\rho\left[\mathrm{kg\,m^{-3}}\right]$	$C_p\left[\mathrm{J\,kg^{-1}K^{-1}}\right]$	$k\left[\mathrm{Wm^{-1}K^{-1}}\right]$	$\sigma\left[\Omega^{-1}\,\mathrm{m^{-1}}\right]$
Water	997.1	4179	0.613	0.005
Diamond	3100	516	1000	34.84×10^6
Cu	8933	385	400	5.96×10^7

method (QLM)", which is an approximation technique to the "*Newton–Raphson method*", was introduced by Bellman and Kalaba (1965) for solving nonlinear equations. The SQLM process begins with the generation of an iterative scheme through the linearizing the nonlinear factors of the ODEs utilizing Taylor approximations in a series form. The "*Chebyshev-spectral collocation method*" is then deployed to solve the computed iterations simultaneously with the overlapping sub-intervals. A comprehensive description of applying the grid and SQLM for the existing nonlinear system for the coupled ODEs is providing below. Exploiting the QLM, the linear system for the set of Eqs. (8)–(10) is given as follows:

$$\alpha_{0,k} f'''_{k+1} + \alpha_{1,k} f''_{k+1} + \alpha_{2,k} f'_{k+1} + \alpha_{3,k} f_{k+1} + \alpha_{4,k} h'_{k+1} + \alpha_{5,k}\theta_{k+1} = Q_{1,k} \tag{16}$$

$$\beta_{0,k} h''_{k+1} + \beta_{1,k} h'_{k+1} + \beta_{2,k} h_{k+1} + \beta_{3,k} f''_{k+1} + \beta_{4,k} f'_{k+1} + \beta_{5,k} f_{k+1} = Q_{2,k} \tag{17}$$

$$\delta_{0,k}\theta''_{k+1} + \delta_{1,k}\theta'_{k+1} + \delta_{2,k}\theta_{k+1} + \delta_{3,k} f'_{k+1} + \delta_{4,k} f_{k+1} = Q_{3,k} \tag{18}$$

where the variable coefficients in Eqs. (16–18) are given as:

$$\left.\begin{aligned}
&\alpha_{0,k} = \frac{1}{A_2}(A_1 + K), \quad \alpha_{1,k} = f_k,\ \alpha_{2,k} = -2f'_k - \frac{1}{A_2}A_3 M - \frac{1}{A_2}A_1 Kp - 2Frf'_k\\
&\alpha_{0,k} = \frac{1}{A_2}(A_1 + K), \quad \alpha_{1,k} = f_k,\ \alpha_{(2,k)} = -2f'_k - \frac{1}{A_2}A_3 M - \frac{1}{A_2}A_1 Kp - 2Frf'_k,\\
&\alpha_{3,k} = f''_k,\ \alpha_{4,k} = \frac{1}{A_2}K,\ \alpha_{4,k} = \frac{A_4}{A_2}Gr,\ \beta_{1,k} = \frac{1}{A_2}\left(A_1 + \frac{K}{2}\right),\ \beta_{(2,k)} = -2\frac{K}{A_2} - f'_k,\\
&\beta_{3,k} = -\frac{K}{A_2},\ \beta_{4,k} = -h_k,\ \beta_{5,k} = f_k\prime,\ \delta_{0,k} = A_5 + \frac{4}{3}Rd + PrA_6\Omega f'^2_k\\
&\delta_{1,k} = PrA_6\Omega f_k f'_k + PrA_6 f_k,\ \delta_{2,k} = B,\ \delta_{(3,k)} = PrA_6\Omega f'_k\theta'_k + A,\\
&\delta_{4,k} = PrA_6\Omega f'_k\theta'_k + 2PrA_6\Omega f_k\theta''_k + PrA_6\theta_k\prime
\end{aligned}\right\} \tag{19}$$

The right-hand side of Eqs. (16–18) are defined as:

$$\left.\begin{aligned}
Q_{1,k} &= \alpha_{0,k} f'''_k + \alpha_{1,k} f''_k + \alpha_{2,k} f'_k + \alpha_{3,k} f_k + \alpha_{4,k} h'_k + \alpha_{5,k}\theta_k - \Lambda_f\\
Q_{2,k} &= \beta_{0,k} h''_k + \beta_{1,k} h'_k + \beta_{2,k} h_k + \beta_{3,k} f''_k + \beta_{4,k} f'_k + \beta_{5,k} f_k - \Lambda_h\\
Q_{3,k} &= \delta_{0,k}\theta''_k + \delta_{1,k}\theta_k\prime + \delta_{2,k}\theta_k + \delta_{3,k} f_k\prime + \delta_{4,k} f_k - \Lambda_\theta
\end{aligned}\right\}$$

where,

$$\left.\begin{aligned}
\Lambda_f &= \frac{1}{A_2}(A_1 + K) f'''_k - f'^2_k + f_k f''_k + \frac{1}{A_2}\left(Kh'_k - A_3 M f'_k + A_1 Kp f'_k\right) + \frac{A_4}{A_2}Gr\theta_k - Frf'^2_k\\
\Lambda_h &= \frac{1}{A_2}\left(A_1 + \frac{K}{2}\right)h''_k - \frac{K}{A_2}\left(2h_k + f''_k\right) + f_k h'_k - f'_k h_k\\
\Lambda_\theta &= \left(A_5 + \frac{4}{3}Rd\right)\theta''_k + \Pr A_6\left(\Omega\left(f_k f'_k\theta'_k + f^2_k\theta''_k\right) + f_k\theta'_k\right) + Af'_k + B\theta_k
\end{aligned}\right\}$$

To initiate the process of SQLM, the partitioned domain for the equations $[0, \infty)$ is first truncated into a adequate region $[0, \eta_\infty]$, where η_∞ represents a limited value chosen to enable the infinity (∞) boundary.

Next, this $[0, \eta_\infty]$ limited domain is uniformly divided into ω subdomains, with each subdomain overlapping the adjacent subdomains by one grid point. These overlapping subdomains are given by:

$$R_\tau = \left[\eta_0^\tau, \eta_q^\tau\right], \tau = 1, 2, 3, \ldots., \omega,$$

where η_0^τ and η_q^τ are the end points of sub-domain presented in R_τ.

In the implementation of the overlapping grid SQLM, each of the sub-domain is discretized utilizing same number of collocation points of Chebyshev rule, which is set to $q+1$. The Chebyshev spectral collocation method employed here relies on a linear transformation, which necessitates that all the sub-intervals have the same length $l = \frac{\eta_\infty}{\omega + \frac{1}{2}(1-\omega)\left(1-\cos\left\{\frac{\pi}{q}\right\}\right)}$. The first two collocation points in the quadrature require the next sub-interval $(R_\tau + 1)$ those are aligned with the collocation points leading to the end of the two of the previous sub-interval (R_τ). This alignment ensures the solution's continuity across the overlapping regions of the sub-intervals.

Since the "spectral collocation method" is effective only in $[-1, 1]$, it is necessary to rescale each sub-domain into the $[-1, 1]$ range with finite sub-intervals. To achieve this, the physical coordinate $\eta \in \left[\eta_0^\tau, \eta_q^\tau\right]$ within the sub-intervals of R_τ, is then distorted several discritized $\breve{\eta} \in [-1, 1]$ range using specific rule defined as

$$\breve{\eta} = \frac{2}{\eta_q^\tau - \eta_0^\tau}\eta - \frac{\eta_q^\tau - \eta_0^\tau}{\eta_q^\tau - \eta_0^\tau}.$$

The Gauss–Lobatto quadrature rule is employed for the collocation nodes in the τ^{th} sub-interval and defined in Canuto et al. (1988) by $\left\{\breve{\eta}_m\right\}_{m=0}^{q} = \cos\left\{\frac{m\pi}{q}\right\}$.

Further, univariate Lagrange interpolating polynomial is used for the function $f(\eta)$ to aapproximate it and presented as;

$$f(\eta) \approx F(\eta) = \sum_{i=0}^{q} F(\eta_i) L_i(\eta). \tag{20}$$

In Eq. (20), $f(\eta)$ is evaluated at specific grid points η_i, where the basis function $L_i(\eta)$ represents the Lagrange cardinal polynomials. A crucial step in applying the spectral method is deriving the differential matrix, which is essential for accurately approximating the derivatives of the unknown functions. However, the differentiation of $f(\eta)$ at the particular collocation points $\left(\breve{\eta}\right)$ in R_τ is given by:

$$\frac{df}{d\eta} \approx \sum_{m=0}^{q} F(\eta_m) L'_m(\eta_r) = \sum_{r=0}^{q} \boldsymbol{D}_{m,r}^{(\tau)} F(\eta_r) = \mathbf{D}^{(\tau)}\mathbf{F},$$
$$m = 0, 1, 2, 3, \cdots, q, \ \tau = 0, 1, 2, 3, \cdots, \omega. \tag{21}$$

In the above, $D_{m,r}^{(\tau)} = \frac{2}{l}\overline{D}_{m,r} (0 \le m, r \le q)$ represents the $(N+1) \times (N+1)$ matrix in the τ^{th} sub-interval which is generally called Chebyshev differential matrix. Here, $N = q + (q-1)(\omega - 1)$ denotes the accumulated grid points participated in computational domain. The vector $\boldsymbol{F} = \left[f\left(\eta_0^\tau\right), f\left(\eta_1^\tau\right), \cdots, f\left(\eta_q^\tau\right)\right]^T$ is the $(q+1) \times 1$ matrix constructed for each node in R_τ, with T indicating the transpose. The matrix $\overline{\boldsymbol{D}}_{m,r} (0 \le m, r \le q)$, which is of order $(q+1) \times (q+1)$ on the interval $[-1, 1]$. The s^{th} order "Chebyshev differential matrices" for the entire domain is calculated through matrix multiplication as shown below:

$$\frac{d^2 f}{d\eta^2} \approx \boldsymbol{D}^2\overline{\boldsymbol{F}}, \frac{d^3 f}{d\eta^3} \approx \boldsymbol{D}^3\overline{\boldsymbol{F}}, \frac{d^s f}{d\eta^s} \approx \boldsymbol{D}^s\overline{\boldsymbol{F}},$$

where $\overline{\boldsymbol{F}} = \left[f(\eta_0), f(\eta_1), \cdots, f\left(\eta_q\right)\right]^T$ of size $(N+1) \times 1$ over the whole computational domain. A similar procedure is employed to approximate the other unknown functions $h(\eta)$ and $\theta(\eta)$. By applying the spectral collocation method and utilizing the discrete derivatives in Eqs. (16) – (18), we obtain the $3(N+1)$ matrix equations with $3(N+1)$ unknowns which can be written in matrix system form as:

$$\begin{bmatrix} A_{11} & A_{12} & A_{13} \\ A_{21} & A_{22} & A_{23} \\ A_{31} & A_{32} & A_{33} \end{bmatrix} \begin{bmatrix} \overline{\mathbf{F}} \\ \overline{\mathbf{H}} \\ \overline{\mathbf{2}} \end{bmatrix} = \begin{bmatrix} \mathbf{Q}_1 \\ \mathbf{Q}_2 \\ \mathbf{Q}_3 \end{bmatrix}, \tag{22}$$

where

$$A_{11} = \left[\alpha_{0,k}\boldsymbol{D}^3 + diag\left[\alpha_{1,k}\right]\boldsymbol{D}^2 + diag\left[\alpha_{2,k}\right]\boldsymbol{D} + diag\left[\alpha_{3,k}\right]\right]\overline{\boldsymbol{F}},$$

$$A_{12} = \left[\alpha_{4,k}\right]\boldsymbol{D}\overline{\boldsymbol{H}}, \ A_{13} = \left[\alpha_{4,k}\right]\overline{\mathbf{2}}$$

$$A_{21} = \left[\beta_{3,k}\boldsymbol{D}^2 + diag\left[\beta_{4,k}\right]\boldsymbol{D} + diag\left[\beta_{5,k}\right]\right]\overline{\boldsymbol{F}}$$

$$A_{22} = \left[\beta_{0,k}\boldsymbol{D}^2 + diag\left[\beta_{1,k}\right]\boldsymbol{D} + diag\left[\beta_{2,k}\right]\right]\overline{\boldsymbol{H}}, \ A_{23} = 0$$

$$A_{31} = \left[diag\left[\delta_{3,k}\right]\boldsymbol{D} + diag\left[\delta_{4,k}\right]\right]\overline{\boldsymbol{F}}, \ A_{32} = 0$$

$$A_{33} = \left[diag\left[\delta_{0,k}\right]\boldsymbol{D}^2 + diag\left[\delta_{1,k}\right]\boldsymbol{D} + \delta_{2,k}\right]\overline{\mathbf{2}},$$

and $diag$ is a diagonal matrix. The surface conditions are approximated at each nodal point. Moreover, iteration process is required for the solution of Eq. (22) to get desired numerical results. The guess solutions chosen that satisfy the proposed surface conditions (11) are utilized to initiate the iteration process. The initial guesses chosen for the model under investigation are:

$$f_0(\eta) = 1 - e^{-\eta},\ h_0(\eta) = ne^{-\eta},\ \theta_0(\eta) = e^{-\eta}.$$

4 Results and discussions

The main aim of the proposed section is to analyse and assess the impact of different variables on profiles such as fluid velocities and temperature, along with other significant material properties. Further, overlapping SQLM is utilized for the numerical simulations of the coupled system of ODEs. To achieve the convergent results, suitable guess functions and a range of physical parameter values are meticulously chosen and adjusted as needed. Results were generated through MATLAB codes, illustrate flow profiles under different physical parameters. The number of collocation points was maintained at a constant value of $N = 30$, except where specified otherwise, and the main domain was divided into five overlapping subintervals.

To ensure the validity and accuracy of the computational method, the numerical results were compared with those reported in previous studies (Mishra et al. 2016). The consistency between our findings and the existing literature confirms the reliability of the numerical approach and the accuracy of the code.

To demonstrate the convergence of the solution method, we examined the solution errors, which highlight the differences between estimated function values across iterations. The convergence is shown using the infinity norm in Table 3, which indicates a steady decrease in convergence errors, confirming the effectiveness of the numerical scheme.

Additionally, the accuracy of the solution approach was evaluated by examining the residual errors of the functions after a specified number of iterations. This involved substituting the approximate solutions into Eqs. (8)–(10) and computing the infinity norm of the residual error, as shown in Table 4. The table reveals a consistent decrease in residual errors for velocities, and temperature profiles. The magnitudes of the residual error values indicate the accuracy of the numerical solution, with lower error norms corresponding to a more accurate solution. Even at the first iteration, the error norms are relatively small, suggesting a good initial guess and rapid convergence. By the 10^{th} iteration, the error norms have further decreased significantly, indicating a high degree of accuracy in the solution profiles for velocities and temperature.

Table 3 Convergence error

Iterations	E_f	E_h	E_θ
1	6.473×10^{-1}	1.530×10^{-1}	7.978×10^{-1}
2	5.487×10^{-3}	3.350×10^{-3}	1.454×10^{-2}
3	3.213×10^{-5}	6.280×10^{-5}	4.836×10^{-4}
4	4.631×10^{-9}	2.210×10^{-9}	3.452×10^{-8}
5	5.218×10^{-15}	2.931×10^{-14}	8.493×10^{-15}
6	3.086×10^{-15}	2.487×10^{-14}	2.498×10^{-15}
7	1.610×10^{-15}	5.551×10^{-15}	4.552×10^{-15}
8	6.273×10^{-15}	7.327×10^{-15}	5.385×10^{-15}
9	5.274×10^{-15}	3.331×10^{-15}	4.430×10^{-15}
10	2.331×10^{-15}	1.554×10^{-15}	2.387×10^{-15}

Table 4 Residual error

Iterations	$\|Res(f)\|_\infty$	$\|Res(h)\|_\infty$	$\|Res(\theta)\|_\infty$
1	9.685×10^{-5}	9.381×10^{-4}	4.460×10^{-4}
2	4.439×10^{-7}	3.521×10^{-5}	5.657×10^{-5}
3	1.561×10^{-11}	7.810×10^{-10}	2.652×10^{-9}
4	5.742×10^{-15}	1.244×10^{-15}	3.352×10^{-15}
5	2.812×10^{-15}	1.113×10^{-15}	2.204×10^{-15}
6	7.490×10^{-15}	1.193×10^{-16}	7.329×10^{-15}
7	7.352×10^{-15}	1.461×10^{-16}	5.341×10^{-16}
8	8.790×10^{-15}	5.765×10^{-17}	6.165×10^{-16}
9	3.157×10^{-15}	6.090×10^{-17}	4.480×10^{-16}
10	9.192×10^{-15}	8.900×10^{-17}	2.598×10^{-16}

5 Validation with parametric behavior

A hybrid micropolar nanofluid combined with diamond and Cu nanomolecules in the base liquid H_2O via a stretching surface filled within a porous substances is presented. The free convective circulation with the interaction of thermal buoyancy, Darcy-Forchheimer inertial drag along with radiating energy and irregular heat sink/source energies the study. The utility of the nanomolecules in combination with the thermophysical models enhance the flow properties. The transmuted set of equations are handeled by utilizing spectral quasilinearization method with the help of the fixed values of the terms intricate in the flow phenomena. The validatioas well as the comparison of the numerical results obtained for the shear aret in particular case is obtainable in Table 5 and Fig. 2. The numerical outputs are compared with the work of Mishra et al. (2016) and these are correlated to each other showing

Table 5 Comparison table of $Re_x^{1/2} C_f$ for different values of K when other parameters are zero and $A_1 = A_2 = 1$

K	Mishra et al. (2016)	Present
0	−1.0000082	−1.000008374
1	−1.3679963	−1.367996272
2	−1.6215752	−1.621575045
3	−1.8273822	−1.827382163
4	−2.0054204	−2.005420369

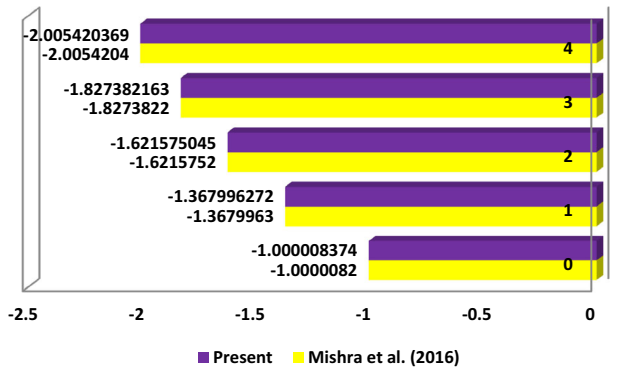


Fig. 2 Validation with previous study for various values of K

the convergence property of the methodology adopted. Further, the variation of each of the factors are depicted through graphs and described in details with their physical significance in the following section. The variation of the factors like inertial drag, magnetic parameter, porosity, surface condition parameter, space dependent heat source/sink, thermal radiation, rotational parameter, and micropolar parameter is presented on the axial velocity, rotational velocity, and the temperature distribution is presented through Figs. 3, 4, 5, 6, 7, 8, 9, 10, 11, and 12. The computation is obtained by considering prandtl number $\mathrm{Pr} = 6.9$ throughout.

The Darcian-Forchheimer inertial drag which is the combination of the Darcy model as well as Forchheimer model on the axial velocity distribution is depicted in Fig. 3. The variation is presented in three distinct profiles such as considering the base liquid water, water based copper nanofluid and the water based diamond and copper hybrid nanofluid. To execute the deviations, the factor is projected within the numerical range of $0 \leq Fr \leq 5$. Here, $Fr = 0$ siginifies the non-existence of the drag force and the non-zero values of Fr shows its effect on the velocity profile. In the base fluid water, for the low value i.r. with zero assigned value of Fr, the flow is primaryly governed by the Darcy law exhibiting linear drag force. The fluid velocity shows a parabolic nature with maximum velocity away from the sheet region. As Fr increases, the inertial effect become more significant. The nonlinear resistance offered by the drag leading to flatetrning

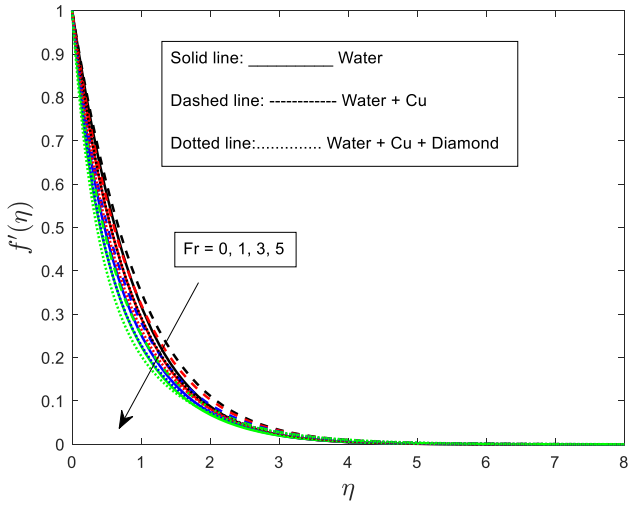


Fig. 3 Influence of Fr on $f\prime(\eta)$

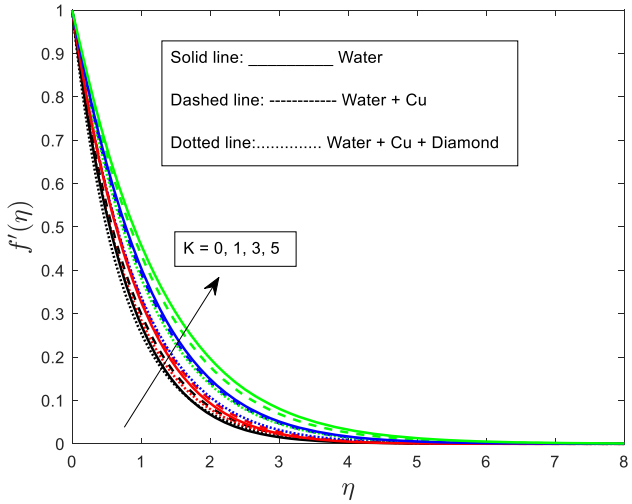


Fig. 4 Influence of K on $f\prime(\eta)$

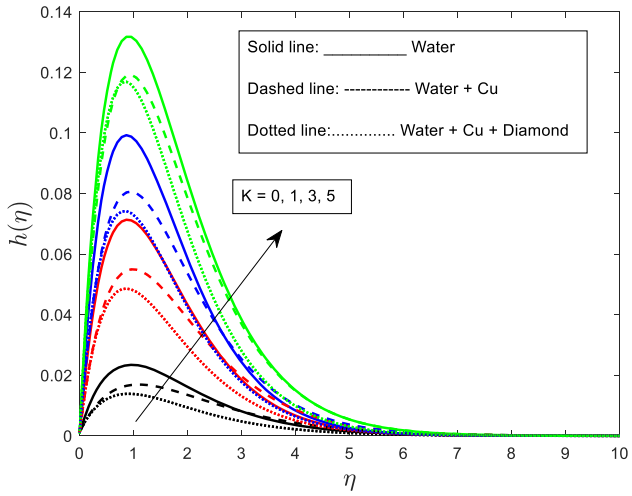


Fig. 5 Influence of K on $h(\eta)$

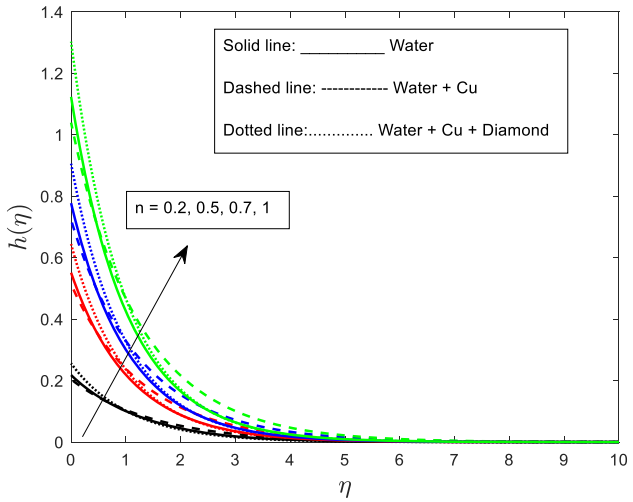


Fig. 6 Influence of n on $h(\eta)$

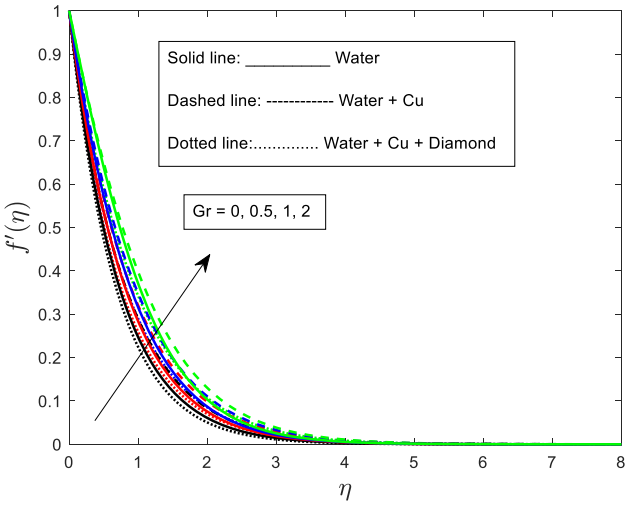


Fig. 9 Influence of Gr on $f\prime(\eta)$

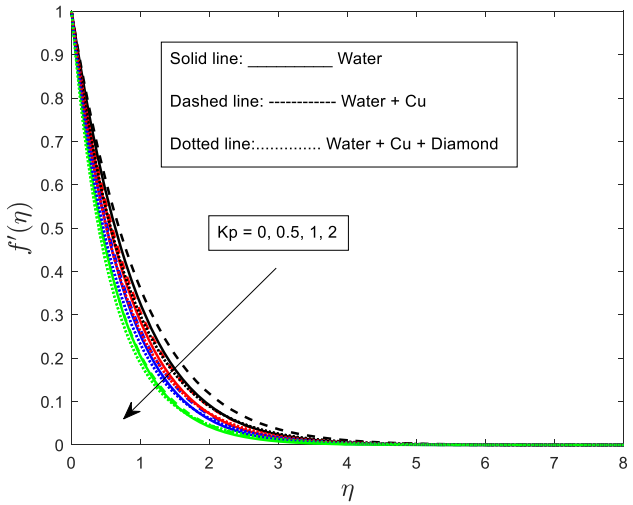


Fig. 7 Influence of Kp on $f\prime(\eta)$

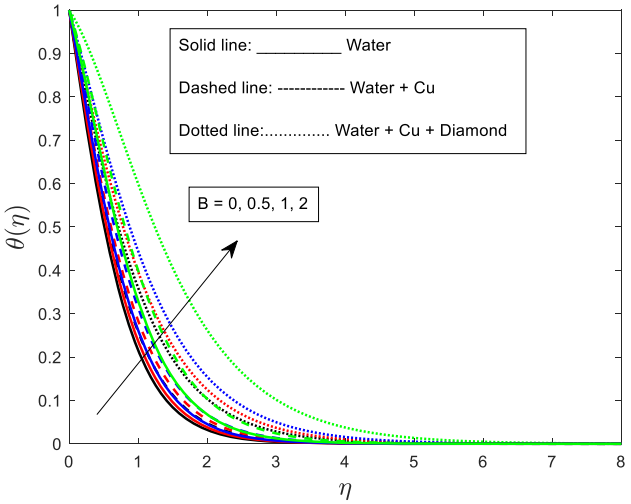


Fig. 10 Influence of B on $\theta(\eta)$

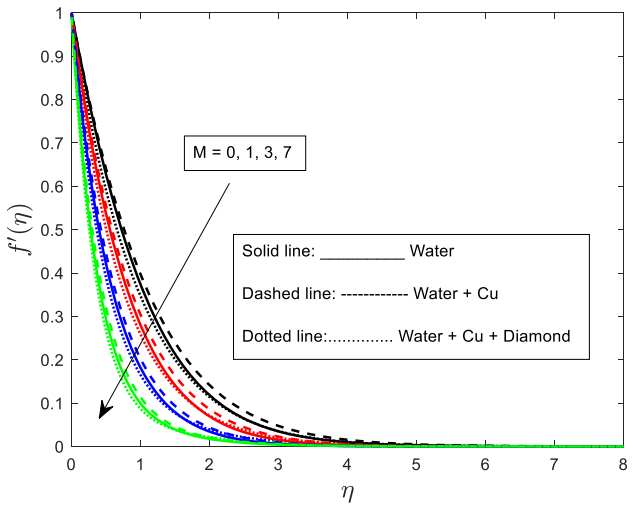


Fig. 8 Influence of M on $f\prime(\eta)$

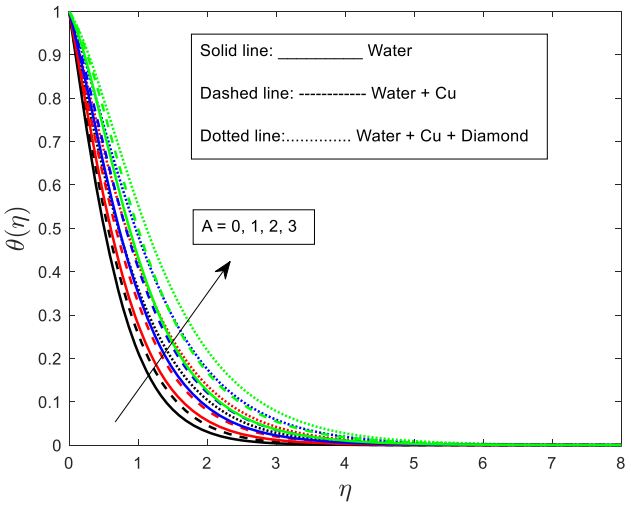


Fig. 11 Influence of A on $\theta(\eta)$

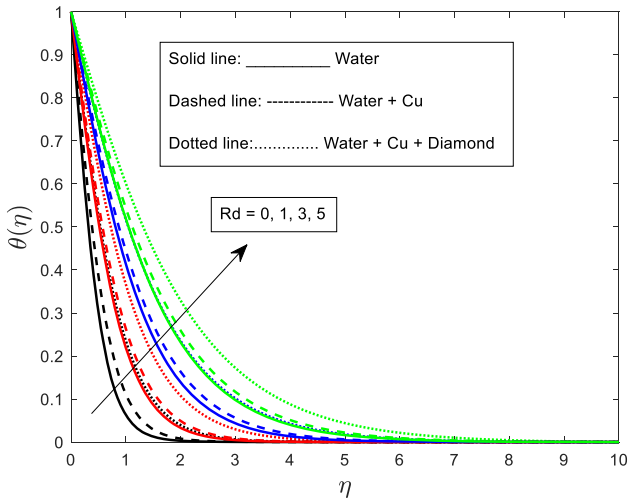


Fig. 12 Influence of Rd on $\theta(\eta)$

of the velocity distribution. This causes a significvant retardation in the fluid velocity. The inclusion of Cu nanoparticles, increases the effective viscosity and for the increase in Fr the reduction is more pronounced. However, the interaction of diamond nanoparticle in the Cu ~ water nanofluid again decelerates the fluid velocity and this retardation is due to the agglomeration of the solid nanoparticle near the surface region.

The motion of micropolar fluid shows its non-Newtonian behaviour for the impact of material parameter (K). The behaviour of the material parameter on the axial fluid velocity is exhibited in Fig. 4. The variation is presented considering the factor within a standard range of $0 \leq K \leq 5$. The numerical result of the parameter $K = 0$ specifies the Newtonian behaviour of the fluid and the non-zero values shows the behaviour considering the case of non-Newtonian fluid. As the material parameter described as the ratio of the vortex viscosity with fluid viscosity, the absence of vortex viscosity lead to the Newtonian behaviour. It is disclosed that the Newtonian fluid lower down the fluid velocity in comparison to the scenario of non-Newtonian fluid. Therefore, increasing the material parameter enhances the fluid velocity throughout and the profile is asymptotically met the requisite surface conditions. The comparative analysis brings stronger relation between the flow through the base fluid and the nanofluid as well as hybrid nanofluid. The velocity decelerates with increasing interaction of one or more solid nanoparticles and it is due to the aggregation and the sedimentation of the nanoparticle closer to the surface region. Figure 5 elaborates the variation of material parameter on the micro rotational profile considering three distinct fluids. The variation shows a sudden hike in the profile near the surface and further it retards sharply. However, the enhanced vales of the micropolar parameter enhance the profile significantly. In connection to the comparison of the profile with respect to the variation of fluids it is observed that the inclusion of more than one nanoparticle the amount of reduction is greater than that of pure as well as nanofluid.

Figure 6 illustrates the wall surface condition on the profile of microrotation for various fluids like base liquid water, nanofluid, hybrid nanofluid. To elaborate the behaviour, the range of the parameter is considered as $0.2 \leq n \leq 1$. In the base liquid water, for $n = 0.2$, the wall condition is relatively smooth leading to lower microrotation velocity near the surface of the fluid. with increasing value of the wall condition, the profile is more pronounced than that of lower value. However, increasing n the profile moves away from the surface showing greater velocity within the domain. In similar, the inclusion of single nanoparticle or more than one nanoparticle the enhancement is quite rigorous and therefore the profile of microrotation increases with the increase of wall condition.

The flow through permeable medium is one of the important assumptions of the study since it has several recent applications for the flow of micropolar fluid. Figure 7 contributes the importance of the permeability of the porous matrix on the profile axial velocity for different fluids. The numerical values adopted for the variation of porosity as borrowed from the earlier literatures as $0 \leq Kp \leq 2$ where the assigned zero value suggests the flow through clear fluid and the nonzero values projects the behaviour of the permeability. The interaction of porosity exhibits a resistive force which shows a retarding effect of the profile of fluid velocity. In either of the considered fluid, the resistance to the flow increases in a porous medium, therefore the flow resistance increases leading to a reduced axial velocity profile across the axial velocity. In comparison to the fluid conditions, hybrid nanofluid exhibits greater retardation than that of the nanofluid and the base liquid water. The fact is that with the inclusion of one or more nanoparticles the density of the fluid increases which causes a agglomeration of the solid particles near the surface and this causes a significant retardation of the profile.

The fluid flow phenomena are affected by the inclusion of the transverse magnetism which is applied along the normal direction of the main flow. Figure 8 displays the imposition of magnetization that affect the axial fluid velocity in the presence of several consideration of the fluids. The range of the parameter M is restricted as $0 \leq M \leq 2$. The considered magnetization $M = 0$ implies the non-existence of the magnetic impact on the flow profiles whereas the nonzero values indicate the role of magnetic parameter on the fluid velocity. The inclusion of the magnetization generally produces a resistive force. This resistive force is due to the occurrence of Lorentz force in general and the impact of this force is to resists the fluid motion. The similar approach is presented in the corresponding profile where the enhanced magnetization reduces the velocity field of the micropolar fluid irrespective

to the nanofluid and the hybrid nanofluid. As discussed earlier the hybrid nanofluid has rendered a greater retardation so that the profile thickness and the bounding surface thickness retards significantly.

The free convection effect is presented on the flow profiles is due to the interaction of the gravitational force. The association of thermal Grashof number is presented on the axial fluid velocity in Fig. 9. The behavior is depicted without the loss of generality of the type of fluid considering within the range of $0 \leq Gr \leq 2$. For $Gr = 0$, the flow is primarily driven by the external force such as pressure gradients, with minimal natural convection effects. However, for the increasing Gr, the flow profiles enhance and this enhancement is irrespective to the type of fluids. The upward force is due to the pressure difference between the various layers of the fluid. This pressure difference is because of the density variation within the layers. It seems that the pressure at the top dominates the pressure at the bottom which causes buoyancy. Therefore, the fluid velocity moves in the upward direction reflecting a significant hike in the axial velocity distribution.

The temperature profile of the micropolar fluid is affected by several contributing factors like, the non-uniform heat source, thermal radiation, and the Eckert number for the existence of other parameters. Figures 10 and 11 exhibits the structural behavior of the space and temperature dependent heat supplier on the thermal energy field respectively. The space dependent temperature parameter A varies within the range of $A \in [0, 3]$ and the temperature dependent parameter $B \in [0, 2]$. In the base fluid, except a relatively simple temperature distribution for the variation depending upon the heat source. Higher B leads to more pronounced nonlinear effects in the fluid temperature. The presence of Cu nanoparticles enhances the effect of thermal conductivity that leads to more uniform temperature distribution. In case of hybrid nanofluid, this rate of deviation increases and the fluid temperature enhances. The comparative analysis shows a significant enhancement in the case of hybrid nanofluid rather than the scenario of nanofluid and the base fluid. The introduction of the solid nanomolecules enriches the thermal conductivity of the nanofluid which contributes a significant hike in the fluid temperature throughout.

To analyse the characteristic of the thermal radiation on the thermal distribution, Fig. 12 exhibits the details feature considering various fluid. The behavior of the parameter is projected considering the range a $Rd \in [0, 5]$. $Rd = 0$ Signifies the absence of the thermal radiation on the heat transport phenomenon within the fluid which is dominated by the conduction and convection both. Irrespective to the type of fluids, it is observed that for the absence of thermal radiation slower down the fluid temperature causing a thinning in the thermal boundary layer. However, the thermal radiation is the measure of the emitted electromagnetic wave

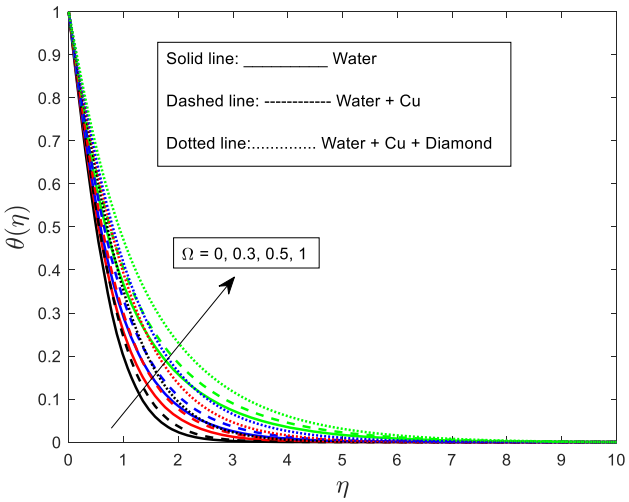


Fig. 13 Influence of Ω on $\theta(\eta)$

from the fluid element which is presented for its nonzero variation within the fluid temperature distribution. This emitted electromagnetic wave further transformed to thermal radiation which causes a significant enhancement in the fluid temperature.

The thermal relaxation parameter plays a significant role on the fluid temperature due to the assumption of the Cattaneo-Christov heat flux model. Figure 13 exhibits the impact of thermal relaxation time on the fluid thermal distribution. The variation of the profile is presented for the suitable consideration of the parameter within the range $0 \leq \Omega \leq 1$. In any of the fluid, Without loss of generality, the consideration Cattaneo-Christov heat flux model give rise to the effect of thermal raelxation factor. Here, $\Omega = 0$ contrubutes the flow behaviuor without the interaction of elasticity terms where the nonzero shows its varation on the fluid temoerature. It is interesting to see that the improved relaxation augments the fluid temoeatyre. As per the earlier variation of the different profiles the hybrid anofluid for the interaction of both Cu and diamond influes the temperature greatly.

Further, the numerical contribution of the various factors on the profile s of shewar rate and heat transfer rate is exhibited and the impact is elaborated clearly. Table 6 shows the role of contributing factor on the shear rate profile keeping certain parameter as fixed. This variation is depicted in three different cases exhibiting its impact on the pure fluid, nanofluid and hybrid nanofluid. The non-Newtonian behavior exhibited by the variation of the material parameter shows that with the enhancement in the microp[olar parameter the skin friction coefficient enhances in magnitude throughout. Further, the buoyancy driven by the thermal convection is deployed and this shows a greater thermal buoyancy decelerates the profile greately. Moreover, the resistivity due to the magnetization and the porosity that declines the fluid

Table 6 Numerical values of skin friction coefficient, $(Re_x)^{1/2}Cf_x$ for different values of K, Gr, Kp, Fr and M when $\phi_1 = 0.01$, $n = 1$, $B = 0.1$, $A = 1$, $Rd = \Omega = 1$, and $\phi_2 = 0.01$

K	Gr	Kp	M	Fr	$Cf_x(H_2O)$	$Cf_x(Cu + H_2O)$	$Cf_x(Cu + H_2O + Diamond)$
0.0	0.5	0.1	1.0	0.1	−2.493700643	−2.601285927	−2.685558038
0.3					−3.201573848	−3.302533800	−3.408354371
0.5					−3.683293373	−3.780119910	−3.899384380
0.5	0.0	0.1	1.0	0.1	−4.290847222	−4.389729198	−4.501383819
	0.5				−3.683293373	−3.780119910	−3.899384380
	1.0				−3.070629774	−3.165460204	−3.294768039
0.5	0.5	0.0	1.0	0.1	−3.581694917	−3.673541373	−3.796047919
		0.3			−3.877430140	−3.983633953	−4.097179145
		0.5			−4.061049792	−4.175980135	−4.284622907
0.5	0.5	0.1	0.0	0.1	−2.451789254	−2.516094367	−2.644174362
			0.5		−3.137413622	−3.219448306	−3.340116242
			1.0		−3.683293373	−3.780119910	−3.899384380
0.5	0.5	0.1	1.0	0.0	−3.618092196	−3.713653149	−3.829919250
				0.3	−3.810181231	−3.909511871	−4.034554738
				0.5	−3.932752074	−4.034550127	−4.165108716

Table 7 Numerical values of Nusselt number, $(Re_x)^{-1/2}Nu_x$ for different values of Rd, Ω, A, and B when $\phi_1 = 0.01$, $n = 1$, $M = 1$, $Fr = 0.1$, $Kp = 0.1$, $Gr = K = 0.5$, and $\phi_2 = 0.01$

Rd	Ω	A	B	$Nu_x(H_2O)$	$Nu_x(Cu + H_2O)$	$Nu_x(Cu + H_2O + Diamond)$
0.0	0.5	0.5	0.1	1.419330452	1.433531093	1.457994083
0.5				1.785720162	1.793655325	1.805618389
1.0				2.063262812	2.067700537	2.071133029
0.5	0.0	0.5	0.1	1.973603650	1.982470088	1.992727682
	0.5			1.785720162	1.793655325	1.805618389
	1.0			1.627265549	1.634461054	1.647706104
0.5	0.5	0.0	0.1	2.027444107	2.038087404	2.048040964
		0.7		1.687611429	1.694470711	1.707287645
		1.0		1.538813840	1.544070259	1.558227088
0.5	0.5	0.5	0.0	1.833161100	1.841740150	1.854904796
			0.3	1.686780163	1.693332251	1.702665576
			0.5	1.581597845	1.586610865	1.592934106

behavior, the velocity gradient decelerates and as a result the shear rate enhances quantitavely. In association with the Darcy-Forchheimer inertial drag also provides a signifiant enhancement in the skin friction coefficient. In all these cases, a compartive analysis is observed between the profile of pure fluid, nanofluid, and the hybrid nanofluid and it is observbed that the rate coefficient enhance gradually in case of hybrid nanofluid. Table 7 displays the variation of the characterizing terms on the heat transfer rate profile. It is revealed that with increasing thermal radiation the heat transfer rate increases sharply and the enhanced values of the thermal realaxation, space and temperature dependent heat source and sink tavors in restricting the heat transfer rate significantly. The tabular result indicates that the heat transfer rate is enhanes for the variation in the water, Cu ~ water and Cu + dimond water hybrid nanofluid.

6 Conclusion

A micropolar hybrid nanofluid comprised of Cu and diamond via an expanding surface with an interaction of radiative heat transfer is deployed in this article. The electrically conducting fluid for the interaction of Darcy-Forchheimer inertial

drag with the impact of non-uniform heat source is exhibited. The transformed model is handled numerically using spectral quasilinearization method and the variation of different factors on the profile is exhibited. The important contribution of several factors on the flow profiles are deployed as;

- The comparison of the contemporary outcomes with the earlier investigation shows a good numerical validation providing the convergence analysis of the proposed methodology.
- The non-Newtonian properties exhibited by the increasing behaviour of the material parameter enhances the axial velocity profile as well as the microrotation.
- The permeability of the medium contributing to the Darcy-Forchheimer inertial drag retards the fluid velocity significantly.
- The resistivity due to the magnetization applied along the normal direction of the flow exhibits attenuation in the fluid velocity but the shear rate enhances greatly.
- The radiative heat due to thermal radiation and the thermal relaxation parameter favors in enhancing the fluid temperature profile.
- The heat transfer rate increases with the variation of the thermal radiation but the thermal relaxation parameter along with the non-uniform heat source retards it.

The proposed study presented for the micropolar fluid can be further extended to design and optimize advanced cooling systems those rae used in microelectronics, The exploration of non-Newtonian fluid coupled with thermal realxation offerd potential applications in drug delivery systems, hyperthermia treatment, etc. The influence of inertial drag, thermal relaxation may enhance enrgy system efficiency.

Author contributions All the authors have equally contributed to complete the manuscript, i.e. TMA has formulated the problem and SP verified the problem statement, SRM has completed the draft with results and discussion section and RB checked the overall.

Funding Not applicable.

Availability of data and material No datasets were generated or analysed during the current study.

Declarations

Conflict of interest The authors declare no competing interests.

Ethical approval The entire work is the original work of the authors.

Consent to participate Not applicable.

Consent for publication All the authors have given their consent to publish the paper.

References

Abbas N, Shatanawi W, Shatnawi TA (2024a) Thermodynamic properties of Casson-Sutterby-micropolar fluid flow over exponential stretching curved sheet with impact of MHD and heat generation. Case Stud Therm Eng 55:104123

Abbas M, Alotaibi H, Muhammad T, Ghazi HM (2024b) A computational framework to explore the impact of heat generation and activation energy on Marangoni convective stagnation point flow of ternary hybrid nanofluid. Adv Mech Eng 16(12):16878132241304602

Abbas M, Ameen HFM, Younis J, Kamolova N, Bonyah E, Ghazi HM (2024c) Computational analysis of thermo-solutal marangoni convective unsteady stagnation point flow of tetra hybrid nanofluid past rotating sphere with activation energy. Int J Thermofluids 25:101025

Abbas M, Marzouki R, Ameen HFM, Dilsora A, Younis J, Akgül A (2024d) Performance of magnetic dipole contribution on electromagnetic Ellis tetra hybrid nanofluid with the applications of surface tension gradient: A Xue model exploration. Int J Thermofluids 24:100951

Abdel-wahed MS, Ahmed SI, Mekheimer KS, Sayed AY (2024) Entropy generation analysis of a micropolar fluid in a corrugated channel with convective and slip conditions. Case Stud Ther Eng 57:104283

Aldhafeeri AA, Yasmin H (2024) Thermal analysis of the water-based micropolar hybrid nanofluid flow comprising diamond and copper nanomaterials past an extending surface. Case Stud Therm Eng 59:104466

Almarashi AM, Algarni A, Rooman M, Shah Z, Garalleh HA (2024) Entropy generation and heat transfer analysis of unsteady micropolar magnetized hybrid-nanofluid flow over a radially stretchable permeable rotating disk with viscous and joule dissipation effects. Int J Thermofluids 23:100802

Anjum N, Khan WA, Hobiny A, Azam M, Waqas M, Irfan M (2022) Numerical analysis for thermal performance of modified Eyring Powell nanofluid flow subject to activation energy and bioconvection dynamic. Case Stud Therm Eng 39:102427

Azeem Khan W (2022) Impact of time-dependent heat and mass transfer phenomenon for magnetized Sutterby nanofluid flow. Waves Random Complex Media. https://doi.org/10.1080/17455030.2022.2140857

Baithalu R, Mishra SR (2023a) On optimizing shear rate analysis for the water-based CNT micropolar nanofluids via an elongating surface: response surface methodology combined with ANOVA test. J Therm Anal Calorim 148(24):14275–14294

Baithalu R, Mishra SR (2023b) On the free convection of magneto-micropolar fluid in association with thermal radiation and chemical reaction and optimized heat transfer rate using response surface methodology. Mod Phys Lett B 37(33):2350171

Baithalu R, Agbaje TM, Mishra SR, Panda S (2024) Diversified characteristics of carbon nanotube nanoparticles on the entropy minimization for the flow of hybrid nanofluid through a convectively heated surface. J Appl Math Mech 104:e202400259

Bellman RE, Kalaba RE (1965) Quasilinearization and nonlinear boundary value problems. RAND corporation, Santa Monica

Canuto C, Hussaini MY, Quarteroni A, Zang TA (1988) Spectral methods in fluid dynamics. Springer, Berlin, p 26

Dharmaiah G, Goud BS, Shah NA, Faisal M (2023) Numerical analysis of heat and mass transfer with viscous dissipation, Joule dissipation, and activation energy. Int J Ambient Energy 44(1):2090–2102

Eid MR, Abd El-Aziz M, Alqarni AJ, Elsaid EM (2024) Numerical analysis for Cattaneo-Christov heat flux on convective viscous non-Newtonian fluid flow through porous medium with nonuniform heat source. Ain Shams Eng J 15:102954

Elboughdiri N, Abbas M, Ayed H, Mouldi A, Fatima N, Abduvalieva D, Galal AM (2024) Numerical simulation of stephan blowing impacts on thermally laminated 3D flow of MHD trihybrid nanofluid with Soret and Dufour effects. Case Stud Therm Eng 66:105460

Faisal M, Ahmad I, Zan-Ul-Abadin Q, Badruddin IA, Hussien M (2024a) Simulation of Casson hybrid nanofluid over bidirectional stretching surface with entropy analysis in stagnated domain. World J Eng. https://doi.org/10.1108/WJE-05-2024-0318

Faisal M, Javed F, Badruddin IA, Ganie AH, Hussien M (2024b) Reiner Rivlin fluid flow between rotatable stretching disks with Cattaneo Christov heat transport. Numer Heat Transfer Part A Appl. https://doi.org/10.1080/10407782.2024.2378182

Goqo SP, Mondal H, Sibanda P, Motsa SS (2019) A multivariate spectral quasilinearisation method for entropy generation in a square cavity filled with porous medium saturated by nanofluid. Case Stud Therm Eng 14:100415

Khan WA (2023) Significance of magnetized Williamson nanofluid flow for ferromagnetic nanoparticles. Waves Random Complex Media. https://doi.org/10.1080/17455030.2023.2207390

Khan WA, Ali M, Irfan M, Khan M, Shahzad M, Sultan F (2020) A rheological analysis of nanofluid subjected to melting heat transport characteristics. Appl Nanosci 10:3161–3170

Khan WA, Arshad Z, Hobiny A, Saleem S, Al-Zubaidi A, Irfan M (2022) Impact of magnetized radiative flow of sutterby nanofluid subjected to convectively heated wedge. Int J Mod Phys B 36(16):2250079

Madkhali HA, Nawaz M, Rana S, Alharbi SO, El-Shafay AS, Ali MR, Hendy AS (2024) Effect of Cattaneo-Christov heat and mass flux in Carreau-Yasuda tri-nanofluid. Case Stud Therm Eng 53:103787

Memon MA, Jacob K, Lanjwani HB, Mahmoud EE (2024) Darcy-Forchheimer MHD micropolar water based hybrid nanofluid flow, heat and mass transfer features past on stretching/shrinking surface with slip and radiation effects. Results Eng 23:102534

Mishra SR, Baag S, Mohapatra DK (2016) Chemical reaction and Soret effects on hydromagnetic micropolar fluid along a stretching sheet. Eng Sci Technol Int J 19(4):1919–1928

Mishra SR, Agbaje TM, Baithalu R, Panda S (2024) Spectral quasilinearization approach for the swimming of motile microorganisms on the bio-convection Casson nanofluid flow over a rotating circular disk. Numer Heat Transfer Part B Fundam. https://doi.org/10.1080/10407790.2024.2352857

Mohapatra R, Panda S, Mishra SR (2024) Exploring heat transfer enhancement: machine learning predictions using artificial neural network for water-based Cu and CuO micropolar nanofluid transportation over a radiating surface. BioNanoScience 14:1–15

Panda S, Ontela S, Mishra SR, Thumma T (2023) Hybridization of artificial neural network and response surface methodology for the optimized heat transfer rate on three-dimensional micropolar nanofluid using Hamilton-Crosser conductivity model through a circular cylinder. J Therm Anal Calorim 148(17):9027–9046

Panda S, Baithalu R, Baag S, Mishra SR (2024) Behaviour of effective heat transfer rate in radiating micropolar nanofluid over an expanding sheet with slip effects. Partial Differ Equ Appl Math 11:100851

Pattnaik PK, Mishra SR, Panda S (2024) Response surface methodology on optimizing heat transfer rate for the free convection of microstructured fluid through permeable shrinking surface. Eur Phys J plus 139(3):221

Ramzan M, Kumam P, Watthayu W (2024) Analyzing heat and mass transport phenomena using the Casson-nanofluid model in the context of Vacuum Pump Oil (VPO) and Cattaneo-Christov heat flux applications. Case Stud Therm Eng 53:103796

Rehman S, Muhammad N, Alshehri M, Alkarni S, Eldin SM, Shah NA (2023a) Analysis of a viscoelastic fluid flow with Cattaneo-Christov heat flux and Soret-Dufour effects. Case Stud Therm Eng 49:103223

Rehman S, Alfaleh A, Afef K, Shah SIA (2023b) Onset about isothermal flow of Carreau liquid over converging channel with Cattaneo-Christov heat and mass fluxes. Heliyon 9(5):e15710

Shamshuddin MD, Panda S, Saeed A, Ratha PK, Mishra SR (2024) Homotopy analysis on magnetized Williamson-micropolar nanofluid flow over a bi-directionally extending surface with multiple slip conditions. Numer Heat Transfer Part B Fundam. https://doi.org/10.1080/10407790.2024.2364783

Upadhya SM, Raju SSR, Raju CSK, Shah NA, Chung JD (2022) Importance of entropy generation on Casson, Micropolar and Hybrid magneto-nanofluids in a suspension of cross-diffusion. Chin J Phys 77:1080–1101

Usafzai WK, Aly EH (2022) Exact multiple solutions of 2-D bidirectional moving plate micropolar hybrid nanofluid flow with heat transfer. Chin J Phys 80:414–426

Vidyarani NJ, Kumar KG, Padmavathi R, Lokesh HJ, Prakasha DG, Kumar VS (2024) Magnetic swirling flow and Cattaneo-Christov heat and mass flux over a stretchable cylinder: a dual stratification model. Ain Shams Eng J 15:102869

Publisher's Note Springer Nature remains neutral with regard to jurisdictional claims in published maps and institutional affiliations.

Springer Nature or its licensor (e.g. a society or other partner) holds exclusive rights to this article under a publishing agreement with the author(s) or other rightsholder(s); author self-archiving of the accepted manuscript version of this article is solely governed by the terms of such publishing agreement and applicable law.